Arch. Metall. Mater. **62** (2017), 2B, 1005-1010

DOI: 10.1515/amm-2017-0142

PEYALA DHARMAIAH*, C.H. LEE, B. MADAVALI, SOON-JIK HONG*#

EFFECT OF SURFACTANT ADDITION ON Bi_2Te_3 NANOSTRUCTURES SYNTHESIZED BY HYDROTHERMAL METHOD

In the present work, we have prepared Bi_2Te_3 nanostructures with different morphologies such as nano-spherical, nanoplates and nanoflakes obtained using various surfactant additions (EG, PVP, and EDTA) by a hydrothermal method. The shape of the nanoparticles can be controlled by addition of surfactants. The samples were characterized by x-ray diffraction (XRD) and scanning electron microscopy (SEM). It is found that the minority BiOCl phase disappears after maintained pH at 10 with EG as surfactant. SEM bulk microstructure reveals that the sample consists of fine and coarse grains. Temperature dependence of thermoelectric properties of the nanostructured bulk sample was investigated in the range of 300-450K. The presence of nanograins in the bulk sample exhibits a reduction of thermal conductivity and less effect on electrical conductivity. As a result, a figure of merit of the sintered bulk sample reached 0.2 at 400 K. A maximum micro Vickers hardness of 102 Hv was obtained for the nanostructured sample, which was higher than the other reported results.

Keywords: Bismuth telluride, hydrothermal synthesis, spark plasma sintering, thermoelectric materials, X-ray diffraction

1. Introduction

More than half the energy consumed nationwide is lost as heat and growing energy demands, concerns over global warming and depleting fossil fuel resources have been the key drivers for the development of sustainable technologies for efficient energy use and recovery of waste energy [1-3]. Thermoelectric (TE) technology involves the direct conversion of waste heat into electricity and vice versa, which can lead to power generation and cooling applications [2]. The performance of TE material is determined by the dimensionless figure of merit $ZT = S^2\sigma T/\kappa$ where S, σ, κ, and T are the Seebeck coefficient, electrical conductivity, thermal conductivity, and absolute temperature, respectively. Slack et al. [4] suggested a new concept of phonon-glass/electron-crystal (PGEC), which states that an efficient thermoelectric material should possess a high σ like a crystalline material and a low thermal conductivity like a glass. A significant research effort has focused on increasing ZT for well known thermoelectric materials by maximizing the Seebeck coefficient and electrical conductivity while minimizing the thermal conductivity. Among them, the reduction of thermal conductivity was an effective strategy for enhancing the *ZT* value higher than 2 [5]. The obtained *ZT* values due to a large number of interfaces in the superlattice structure, which plays a significant role in reducing κ_{lat} by interface phonon scattering.

Bismuth telluride, Bi_2Te_3, and its derivatives are the best TE materials used in the state-of-the-art devices for the 200-400K temperature range. Bulk Bi_2Te_3 based alloys exhibit a *ZT* value close to unity [6]. Theoretical studies showed that making nanostructured bulk TE materials could enhance *ZT* by decreasing their phonon thermal conductivity. During the past decades, there have been many reports on different attempts to enhance the *ZT* values of the nanostructured bismuth telluride based alloys. Hicks et al. [7] showed that the *ZT* value of Bi_2Te_3 quantum well might be higher than the bulk value. X.B. Zhao et al. [8] used the hydrothermal method for preparation of nanotubes and utilized ball milling followed by hot-pressing for producing nanotube containing nanocomposites, which showed a high *ZT* value of 1.05 at 450 K. However, the reported *ZT* values of n-type Bi_2Te_3 still remain below unity compared to p-type Bi_2Te_3 materials. Bi_2Te_3 nanoparticles can be synthesized via methods like co-precipitation [9], reverse micelle [10], microemulsion [11], reduction of metal-organo complexes [12], and hydrothermal (solvothermal) method [13, 14]. Among them, the hydrothermal method has the salient features such as low reaction temperature which leads to fewer crystal defects, and thermal stresses, homogenous reaction conditions resulting in narrow size distribution, simple operation with low cost. Thermoelectric properties strongly influenced by the morphologies of the powder and their sizes [14]. Recently, hydrothermal or solvothermal have been used to prepare various morphologies of Bi_2Te_3 alloys including nano sphericals, polygonal nanosheets, polyhedral nanoparticles and sheet rods [14-16].

In this work, we report on the effects of EG, PVP, and EDTA as surfactants on the surface morphology and thermoelectric properties of spark plasma sintered sample was discussed.

* DIVISION OF ADVANCED MATERIALS ENGINEERING, KONGJU NATIONAL UNIVERSITY, CHEONAN CITY REPUBLIC OF KOREA.

Corresponding author: hongsj@kongju.ac.kr

2. Experimental procedure

In a typical process, high purity (>99.99%, Alfa Aesar Co. Ltd) analytical reagent (AR) grade $BiCl_3$, and Te powder were used as the precursors with a molar ratio of 2:3. Initially, 0.15g Te, 0.25 g $BiCl_3$, 0.5 g surfactants (EG – ethylene glycol, PVP-polyvinylpyrrolidone, or EDTA – ethylenediaminetetraacetic acid), and 1.5 g $NaBH_4$ as the reducing agent were added to 300 mL capacity neck flask containing 150 mL deionized water. The solution was stirred for 10 min by a magnetic stirrer. In the second step, NaOH gradually added to the solution for control the pH value. The solution containing flask was kept in a home-made oil bath setup for maintaining the uniform temperature at 70°C for 12 h with continuous stirring. To investigate the effects of surfactant additives on the morphology of the Bi_2Te_3 nanoparticles, three parallel experiments were performed through a similar route as described above. After completion of reaction time, the system was naturally cooled to room temperature. The resulting dark gray powders were filtered using centrifugation and washed with distilled water, and ethanol for several times and subsequently dried in vacuum oven at 60°C. The resulting powder of EG-pH10 sample was consolidated using spark plasma sintering at 623 K for 10 min under a pressure of 50 MPa in a 20-mm diameter graphite die. The phase structure of the powders was investigated by x-ray diffraction (XRD) with a Rigaku, MiniFlex-600 diffractometer using CuKα radiation at room temperature. The powder morphologies and fracture surface were analyzed using scanning electron microscopy (SEM-MIRA LMH II (TESKAN)). The relative density and Vickers microhardness of the sample were estimated by using the Archimedes method and a Vickers hardness tester, respectively. The Seebeck coefficient (S) and electrical conductivity (σ) were measured using a thermoelectric measurement system (TEP-1000, Seepel). The total thermal conductivity κ was calculated using the equation $\kappa = \lambda C_p d$, where d is the bulk density of the sample, λ is thermal diffusivity, and C_p is the heat capacity, were measured on a Netzch LFA 457 system. The carrier concentration (n_c) and mobility (μ_c) were measured using Hall measurement setup (Ecopia HMS-3000).

3. Results and discussion

XRD patterns of the Bi_2Te_3 nanopowders synthesized with different surfactants are given in Fig. 1. As can be seen in Fig. 1 that the powders synthesized individually using EG, PVP, and EDTA contains Bi_2Te_3 as majority and BiOCl as minority phases could be clearly identified. The formation of minority phase was may be due to the reaction of $BiCl_3$ with H_2O. The BiOCl phase was disappeared after maintained at pH 10 with EG. These results suggest that the single phase of Bi_2Te_3 is difficult to produce with EG, PVP, EDTA surfactant additions; however, a single phase of Bi_2Te_3 was clearly identified after maintaining the pH value at 10. The diffraction peaks could be indexed to reflections of rhombohedral phase Bi_2Te_3 with lattice parameters a = 4.395Å, and c = 30.440 Å (JCPDS#820358). The intense and sharp diffraction peaks from EG-pH10 sample are typical signatures of a high degree of crystallinity. Firstly, Te powder was reduced to Te^{2-} by reducing agent ($NaBH_4$) in the presence of strong alkaline solution (NaOH). The reduced Te^{2-} ions react with Bi^{3+} to form the Bi_2Te_3 nanoparticles during hydrothermal synthesis. The result indicates that strong alkaline

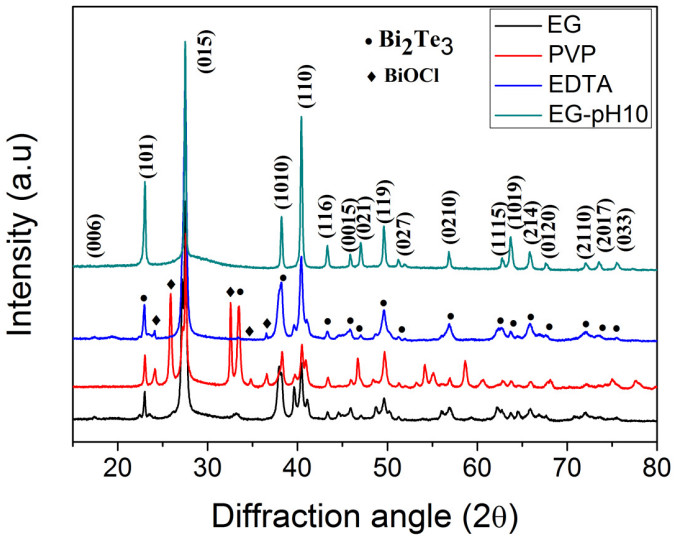

Fig. 1. Powder X-ray diffraction patterns of as-prepared Bi_2Te_3 nanoparticles with different surfactant additions

The morphology of the nanopowders with different surfactant additions are shown in Fig. 2. As can be seen in Fig. 2a, the Bi_2Te_3 nanoparticles obtained using EG as surfactant were spherical in shape and slightly agglomerated with particle size about 25 nm. The fine nanoparticles can be easily agglomerated owing to their high surface energy. The plate-like nanostructures were identified using PVP as surfactant (see Fig. 2b). The size of the nanoparticle is around 200 nm. Nano-flake shape morphology was observed with a length of about 300 nm by using EDTA as surfactant (see Fig. 2c). Interestingly, uniform spherical nanoparticles were observed while maintaining pH at 10, and using EG as surfactant. The results suggest that surfactants can induce the growth manner and direction of the grain to form different morphology. A single phase of Bi_2Te_3 nanopowder was consolidated using spark plasma sintering. The relative density of spark plasma sintered sample was found as 98.95%.

Fig. 3 shows SEM micrographs of a fracture surface of the Bi_2Te_3 bulk sample prepared from EG-pH10 nanopowder. As can be seen in the Fig. 3a, the laminated structure was observed and there is no obvious porosity in the bulk sample. At high magnification clearly, reveals that the bulk fracture consists of fine and coarse grains. It is expected that the combination of fine and coarse grains could be possibly reducing the total thermal conductivity due to the enhanced scattering of phonons by the fine grains.

Fig. 4 shows the temperature dependence of Seebeck coefficient, electrical conductivity and power factor for the EG-pH10 nanostructured bulk sample. As shown in Fig 4(a), The result indicates that strong alkaline medium was essential for forma-

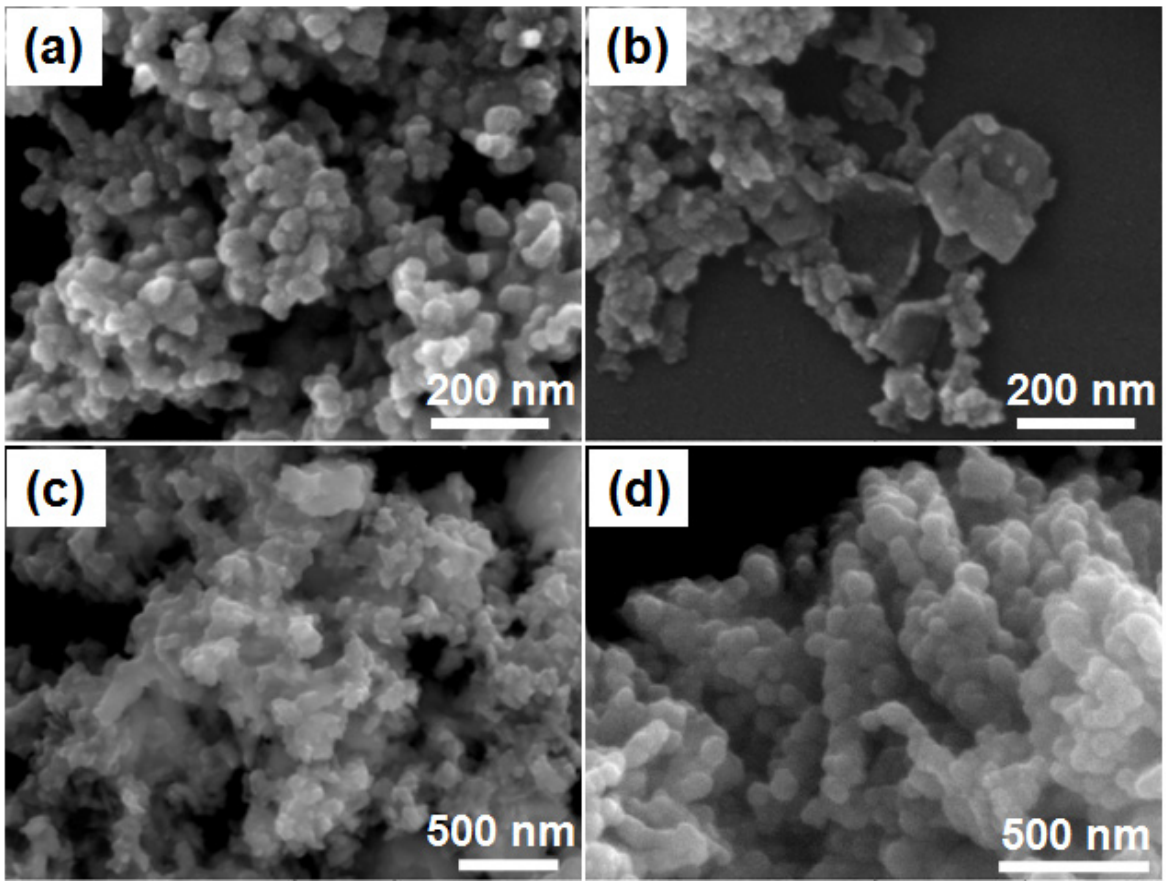

Fig. 2. Scanning electron microscopy images of Bi_2Te_3 nanoparticles prepared using different surfactant additives: (a) EG, (b) PVP, (c) EDTA and (d) EG-pH10

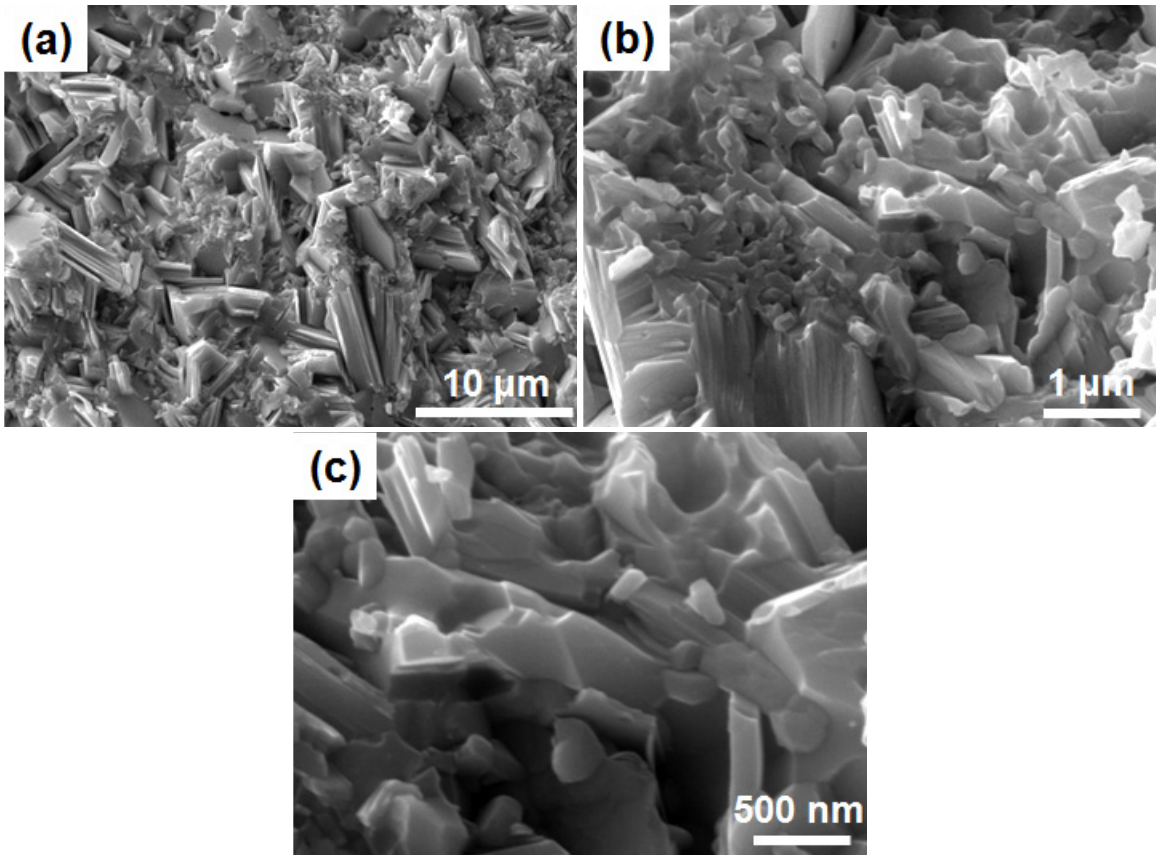

Fig. 3. SEM images of spark plasma sintered samples processed from EG-pH10 nanoparticles (a) low, (b) medium and (c) high magnification

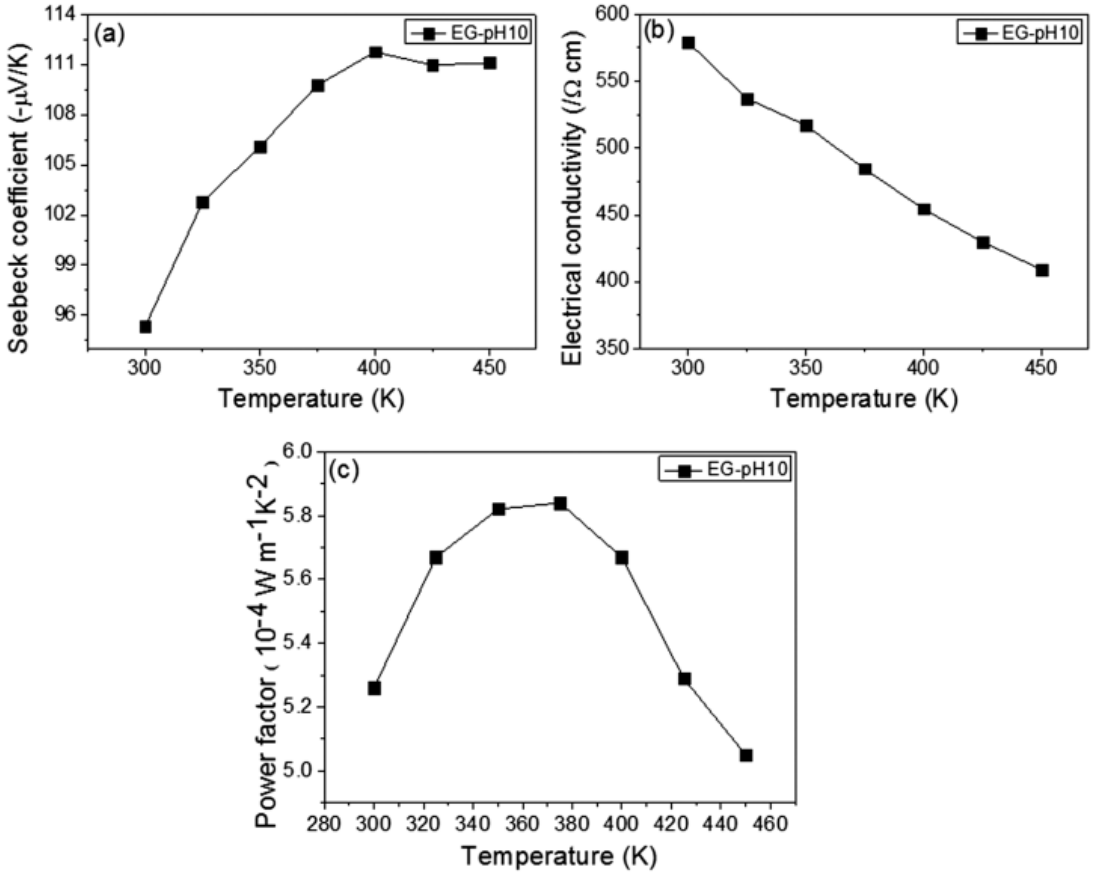

Fig. 4. Temperature dependence of transport properties of the SPS-processed bulk samples (a) Seebeck coefficient; shows an increasing behavior with temperature to a maximum and then slightly decreases with further increase in temperature (b) Electrical conductivity; decreases with temperature indicates degenerate semiconducting nature, (c) Power factor

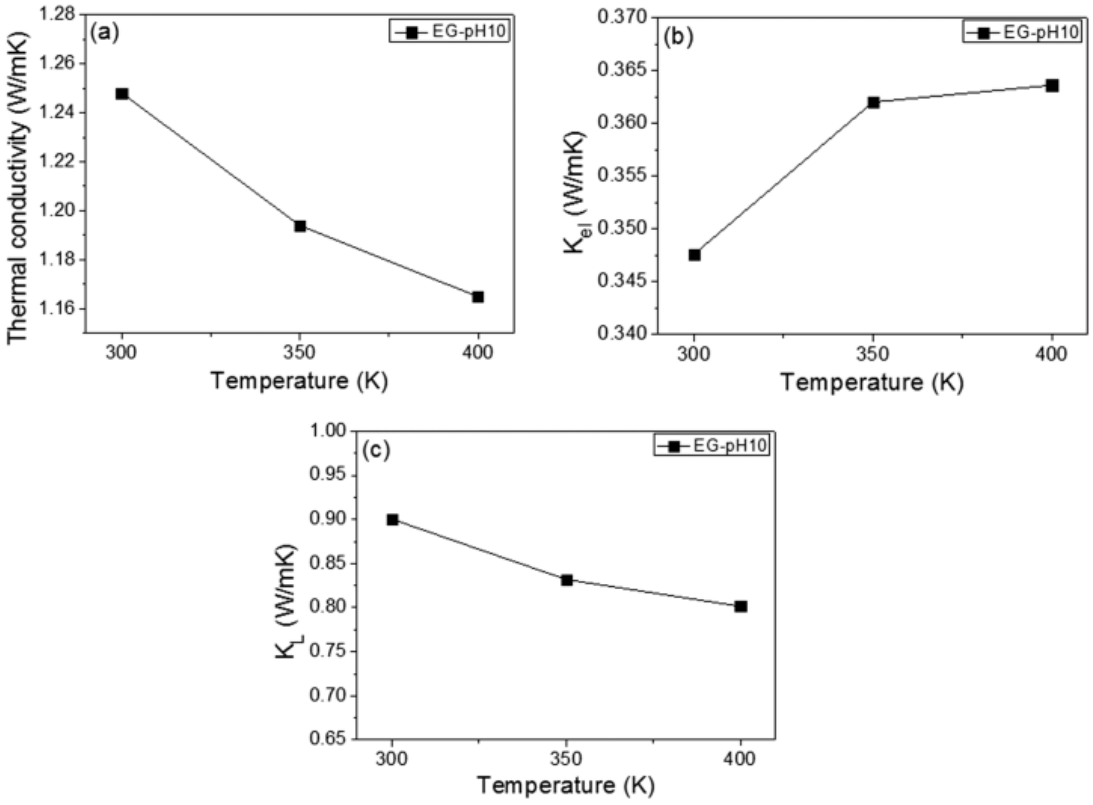

Fig. 5. Temperature dependence of thermal transport properties of the spark plasma sintered bulk sample (a) Total thermal conductivity, (b) Electronic contribution to thermal conductivity, (c) Lattice contribution to thermal conductivity

tion Bi2Te3 nanocrystals the Seebeck coefficient values for the sample shows negative sign which confirms that electrons are the majority carriers in the transportation. The Seebeck coefficient values increase with temperature, it reaches a maximum value of 112 μV/K around 400 K and decreases at higher temperatures due to the intrinsic excitation of minority carriers. It is well known that the Seebeck coefficient can be expressed as Eq. (1)

$$S = \frac{k_B}{e}\left(\gamma + \frac{5}{2} + \ln \frac{2\left(2\pi m^* k_B T\right)^{3/2}}{nh^3} \right) \quad (1)$$

where γ is the scattering parameter, h is Planck's constant, and e is the carrier charge. According to Eq. (1), the S could be increased with the decrease of carrier concentration via the increase of scattering parameter [17].

Fig. 4(b) shows the temperature dependences of electrical conductivity for the EG-pH10 bulk sample. The electrical conductivity values of the sample decrease with increasing measuring temperature, indicating a degenerate semiconducting behavior. The electrical conductivity of EG-pH10 sample was about 579 (/Ωcm) at 300 K which is higher than reported papers [18]. The electrical conductivity (σ) and carrier concentration (n) as well as the mobility (μ) described as $\sigma = ne\mu$. In order to clearly understanding the transport mechanism, we have been measured carrier concentration and mobility using Hall measurement. The carrier concentration and mobility of the bulk sample was measured as 3.69×10^{19} /cm^3 and 97 cm^2/Vs, respectively.

Fig. 4(c) shows the temperature dependences of power factor for the EG-pH10 sintered bulk sample. The power factor can be estimated using measured Seebeck coefficient and electrical conductivity. The maximum value of power factor of 5.85×10^{-4} Wm^{-1}K^{-2} at 375 K was obtained.

The temperature dependences of thermal transport properties for the EG-pH10 sintered bulk samples are presented in Fig. 5. As shown in Fig. 5(a), the total thermal conductivity of EG-pH10 bulk sample exhibited 1.16 W/mK at 400 K. The attained value is lower than the reported thermal conductivity of rare earth containing Bi_2Te_3 binary compounds prepared by the solvothermal process [18]. The thermal conductivity decreases with increase in temperature reveal the dominance of phonon-phonon scattering. The lower thermal conductivity was due to the enhancement of phonon scattering by introducing a lot of grain boundaries through nanometer-sized spherical grains.

The total thermal conductivity is expressed by the sum of a lattice (κ_{ph}), and electronic contributions (κ_{el}). According to Wiedemann-Franz's law, κ_{el} can be estimated as: $\kappa_{el} = L\sigma T$, here L is the Lorenz number taken as 2.0×10^{-8} V^2/K^2 for a degenerate semiconductor [19]. The lattice thermal conductivity κ_{ph} is then estimated by subtracting κ_{el} from κ. The temperature dependence of electronic and lattice thermal conductivity are shown in Fig. 5(b, c).

Fig. 6 shows the dimensionless figure of merit (ZT) as a function of temperature for the EG-pH10 sintered bulk sample. The maximum ZT of 0.2 at 400 K was obtained; which is higher or comparable to that of other Bi_2Te_3 nanostructures synthesized by various solution methods [18]. The mechanical strength of thermoelectric materials is important for preparation TE modules. The maximum Vickers hardness of 102 Hv was obtained for the EG-pH10 sintered sample, which is significantly higher or comparable to several reported results [14,20]. The obtained high hardness in the bulk sample was due to the presence of fine grains and increased amount of grain boundaries [20].

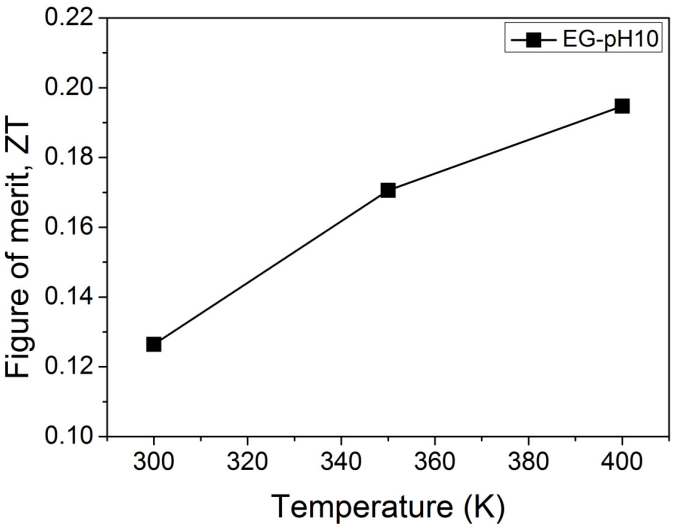

Fig. 6. Temperature dependence of dimensionless figure of merit ZT of the nanostructured bulk sample

4. Conclusions

In summary, we have demonstrated the effect of surfactant addition on the morphology of Bi_2Te_3 nanoparticles. The temperature dependence of thermoelectric properties was systematically investigated. The experimental results reveal that EG-pH10 sample exhibited a single phase of Bi_2Te_3 at present synthesis conditions. The spark plasma sintered bulk sample composed of fine and coarse grains. Such a fine grains can induce a large reduction in the thermal conductivity by enhanced scattering of phonons at grain boundaries. As results, a maximum figure of merit ZT of 0.2 at 400 K was obtained for the EG-pH10 sample. The Vickers microhardness of the sintered samples significantly improved, and comparable with best results found in the literature.

Acknowledgements

This work is supported by the research grant of Kongju National University in 2016.

REFERENCES

[1] G.J. Snyder, E.S. Toberer, Nat. Mater. **7**, 105 (2008).
[2] P. Dharmaiah, H.S. Kim, K.H. Lee, S.J. Hong, Arch. Metall. Mater. **60,** 1417 (2015).

[3] M.S. Dresselhaus, G. Chen, M.Y. Tang, R.G. Yang, H. Lee, D.Z. Wang, Z.F. Ren, J.P. Fleurial, P. Gogna, Adv. Mater. **19**, 1043 (2007).
[4] G.A. Slack, V.G. Tsoukala, J. Appl. Phys. **76**, 1665 (1994).
[5] R. Venkatasubramanian, E. Siivola, T. Colpitts, B. O'Quinn, Nature **11**, 597 (2001).
[6] D.M. Rowe, Thermoelectrics handbook: macro to nano. illustrated ed: CRC Press, Boca Raton; 1995.
[7] L.D. Hicks, M.S. Dresselhaus, Phys. Rev., B **47**,12727-31 (1993).
[8] X.B. Zhao, X.H. Ji, Y.H. Zhang, T.J. Zhu, J.P. Tu, X.B. Zhang, Appl. Phys. Lett. **86**, 062111 (2005).
[9] J.J. Ritter, Inorg Chem. **33**, 6419-20 (1994).
[10] E.E. Foos, R.M. Stroud, A.D. Berry, Nano Lett. **1**, 693-5 (2001).
[11] A. Purkayastha, S. Kim, D.D. Gandhi, P.G. Ganesan, T.B. Tasciuc, G. Ramanath, Adv Mater. **18**, 2958 (2006).
[12] M. Scheele, N. Oeschler, K. Meier, A. Kornowski, C. Klinke, H. Weller, Adv Funct Mater. **19**, 3476-83 (2009).
[13] L.N. Zhou, X.B. Zhang, X.B Zhao, T.J. Zhu, Y.Q. Qin, J Mater Sci. **44**, 3528-32 (2009).
[14] P. Dharmaiah, S.J. Hong, J. Electron. Mater., DOI: 10.1007/s11664-016-5104-2, (2016).
[15] Y. Deng, X.S. Zhou, G.D. Wei, J. Liu, C.W. Nan, S.J. Zhao, J. Phys. Chem. Solids. **63**, 2119 (2002).
[16] X.B. Zhao, Y.H. Zhang, X.H. Ji, Inorg. Chem. Commun. **7**, 386 (2004).
[17] K.C. Park, P. Dharmaiah, H.S. Kim, S.J. Hong, J. Alloys Compd. **692**, 573 (2016)
[18] X.H. Ji, X.B. Zhao, Y.H. Zhang, B.H. Lu, H.L. Ni, J. Alloys Compd. **387**, 282-286 (2005)
[19] W. Xie, X. Tang, Y. Yan, Q. Zhang, T.M. Tritt, Appl. Phys. Lett. **94**, 102111, (2009).
[20] P. Dharmaiah, H.S. Kim, C.H. Lee, S.J. Hong, J. Alloys Compd. **686**, 1 (2016).